





Design of an Efficient Pulsed Dy³⁺: ZBLAN Fiber Laser Operating in Gain Switching Regime

Mario Christian Falconi, *Student Member, IEEE*, Dario Laneve , Michele Bozzetti , Toney Teddy Fernandez, Gianluca Galzerano , and Francesco Prudenzano 

Abstract—A time-dependent numerical model of a dysprosium-doped ZBLAN glass fiber is developed in order to design a pulsed laser emitting at about 3 μm wavelength, by employing an in-band pumping scheme. A number of design parameters are changed to optimize the laser performance. Gain-switching regime with an output signal peak power close to 59 W and a full width at half maximum pulse duration shorter than 184 ns is simulated for a fiber with dopant concentration of 2000 ppm, by employing a pulsed input pump with a peak power of 5 W and a repetition rate of 100 kHz at the wavelength of 2.8 μm . These characteristics are very promising and theoretically predict the feasibility of a laser, which can find application in many areas such as chemical, biological, and environmental monitoring.

Index Terms—Dysprosium, fiber laser, gain switching, middle infrared, ZBLAN glass.

I. INTRODUCTION

THE need for high beam quality ($M^2 \approx 1$) emission in the middle-infrared (Mid-IR) wavelength range is originated by a number of potential applications, in the field of free-space communication, chemical and biological sensing, remote sensing and earth atmosphere monitoring, medical diagnostic and surgery, material processing and material science measurements. More precisely, the interaction of Mid-IR light beams with biological tissues, gases, water, air contaminants and many other materials is extremely promising. Innovative sensing systems can be developed by exploiting the characteristic absorption fingerprints exhibited by the chemical and biological molecules in the Mid-IR wavelength range (2–20 μm) due to, e.g., the vibrational resonances of C-H, N-H and O-H chemical

bonds. Also laser ablation surgery can be efficiently obtained at Mid-IR wavelengths by exploiting the strong water absorption. Novel communication systems based on free space propagation could utilize the transmission windows of earth atmosphere, e.g., the 3–4 μm , 4.3–5.0 μm , 8–10 μm and 10–14 μm wavelength ranges.

Different glasses can be employed as host materials for the construction of rare-earth-doped fiber lasers providing efficient Mid-IR emission. Chalcogenide fiber lasers have been extensively investigated for their excellent transparency at very long wavelengths, till 20 μm , but further technological development is required in order to obtain working prototypes [1]–[8]. Tellurite [9]–[11] and fluoride [12]–[23] fiber glasses constitute more feasible alternatives in the 2–3 μm wavelength range. In particular, the market availability of efficient laser diodes as pumping sources has allowed significant advances in the construction of both continuous-wave (CW) and pulsed ZBLAN fiber lasers close to 3 μm wavelength. As an example, in [24] a Q-switched Er³⁺-doped ZBLAN fluoride fiber laser has been proposed. Nonlinear polarization rotation (NPR) method [25] and gain switching [26]–[28] constitute further approaches in order to obtain high-energy pulsed laser operation.

In this work, for the first time to the best of our knowledge, a time-dependent numerical model for an in-band pumped configuration of Dy³⁺-doped ZBLAN fiber laser is proposed in order to investigate the generation of optical pulses at 3 μm . Till now, only CW Dy³⁺-doped ZBLAN fiber lasers with in-band pumped configuration have been demonstrated [29]–[32]. Therefore, the investigation illustrated in this work could pave the way to the pulsed operation for this kind of lasers. The gain switching method, in which a suitable input pump modulates the optical gain, is considered to achieve pulsed operation. Stable single-pulse regime is predicted. Moreover, this investigation has a practical interest since simulation parameters pertaining to commercially available fluoride fibers are employed [32].

II. GAIN-SWITCHED LASER MODEL

In the proposed model, the rate equations coupled with the time-varying power propagation equations for the pump and signal beams are solved by including the time derivatives. Group velocity for all propagating waves is taken into account [26], [27], [33]. A numerical code based on a modified FDTD approach is implemented. A first-order forward-time scheme is considered for the rate equations [34].

Manuscript received June 29, 2018; revised September 16, 2018; accepted September 17, 2018. Date of publication September 26, 2018; date of current version November 2, 2018. This work was supported in part by the Ministry of Economic Development under Grant Horizon 2020—PON, I&C 2014–2020, research project: “ERHA—Enhanced Radiotherapy with HAdron,” no. F/050425/02/X32, and in part by HORIZON 2020—COST ACTION MP 1401, Advanced Fibre Laser and Coherent Source as Tools for Society, Manufacturing and Lifescience. (*Corresponding author: Francesco Prudenzano.*)

M. C. Falconi, D. Laneve, M. Bozzetti, and F. Prudenzano are with the Department of Electrical and Information Engineering, Politecnico di Bari, 70125 Bari, Italy (e-mail: mariochristian.falconi@poliba.it; dario.laneve@poliba.it; michele.bozzetti@poliba.it; francesco.prudenzano@poliba.it).

T. T. Fernandez is with the MQ Photonics Research Centre, Department of Physics and Astronomy, Macquarie University, Sydney, NSW 2109, Australia (e-mail: toney.teddyfernandez@mq.edu.au).

G. Galzerano is with the IFN-CNR, Department of Physics, Politecnico di Milano, 20133 Milano, Italy (e-mail: gianluca.galzerano@polimi.it).

Color versions of one or more of the figures in this paper are available online at <http://ieeexplore.ieee.org>.

Digital Object Identifier 10.1109/JLT.2018.2871665

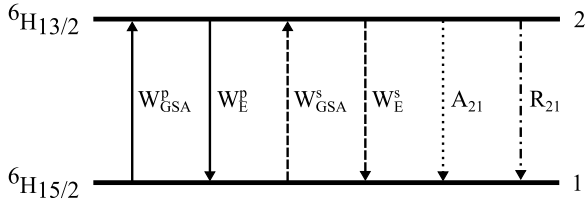


Fig. 1. Dy^{3+} energy levels and transitions for the case of $\lambda_p = 2.8 \mu m$ in-band pumping.

The optical behavior of dysprosium ions, for in-band pumping at $\lambda_p = 2.8 \mu m$ wavelength, can be suitably modeled by employing a two levels laser system, as shown in Fig. 1. The ${}^6H_{15/2}$ and ${}^6H_{13/2}$ energy levels are the fundamental state and the excited state, respectively. By taking into account the typical light-rare earth interactions, i.e., absorption, stimulated emission, radiative and nonradiative decays, the following equation system for the level populations $N_1(x, y, z, t)$ and $N_2(x, y, z, t)$ can be written:

$$\begin{cases} \frac{\partial N_2}{\partial t} = W_{GSA} N_1 - (W_E + A_{21} + R_{21}) N_2 \\ \frac{\partial N_1}{\partial t} = -W_{GSA} N_1 + (W_E + A_{21} + R_{21}) N_2 \end{cases} \quad (1)$$

where $W_{GSA} = W_{GSA}^p + W_{GSA}^s$ is the total transition rate pertaining to the Ground State Absorption (GSA), $W_E = W_E^p + W_E^s$ is the total transition rate pertaining to the Stimulated Emission (E), while $A_{21} = \tau_2^{-1}$ and $R_{21} = T_{21}^{-1}$ are the radiative and nonradiative decay rates for the ${}^6H_{13/2} \rightarrow {}^6H_{15/2}$ transition, respectively. The transition rates for the pump (p) and the signal (s) can be calculated as follows:

$$\begin{aligned} W_{GSA}^p &= \frac{\sigma_{12}(\nu_p)}{h\nu_p} [P_p^+(z, t) + P_p^-(z, t)] i_p(x, y) \\ W_E^p &= \frac{\sigma_{21}(\nu_p)}{h\nu_p} [P_p^+(z, t) + P_p^-(z, t)] i_p(x, y) \\ W_{GSA}^s &= \frac{\sigma_{12}(\nu_s)}{h\nu_s} [P_s^+(z, t) + P_s^-(z, t)] i_s(x, y) \\ W_E^s &= \frac{\sigma_{21}(\nu_s)}{h\nu_s} [P_s^+(z, t) + P_s^-(z, t)] i_s(x, y) \end{aligned}$$

where h is the Planck constant, ν_p is the pump frequency, ν_s is the signal frequency, $\sigma_{12}(\nu)$ and $\sigma_{21}(\nu)$ are the frequency-dependent absorption and emission cross sections, respectively, P_p^\pm is the forward/backward pump power and P_s^\pm is the forward/backward signal power, i_p and i_s are the normalized transverse intensity profiles of pump and signal beams, respectively. The previous system of differential equations (1) can be simplified because the sum of level populations is equal to the total dopant concentration $N_{Dy}(x, y, z) = N_1(x, y, z, t) + N_2(x, y, z, t)$:

$$\begin{cases} \frac{\partial N_2}{\partial t} = W_{GSA} N_1 - (W_E + A_{21} + R_{21}) N_2 \\ N_1(x, y, z, t) = N_{Dy}(x, y, z) - N_2(x, y, z, t) \end{cases} \quad (2)$$

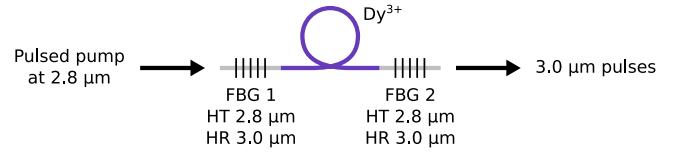


Fig. 2. Schematic of the device.

The propagation of the pump and signal optical beams is taken into account by the following nonlinear partial differential equations:

$$\begin{cases} \frac{\partial P_p^+}{\partial z} + \frac{1}{v_g^p} \frac{\partial P_p^+}{\partial t} = [g_p(z, t) - \alpha(\nu_p)] P_p^+ \\ \frac{\partial P_p^-}{\partial z} - \frac{1}{v_g^p} \frac{\partial P_p^-}{\partial t} = [-g_p(z, t) + \alpha(\nu_p)] P_p^- \\ \frac{\partial P_s^+}{\partial z} + \frac{1}{v_g^s} \frac{\partial P_s^+}{\partial t} = [g_s(z, t) - \alpha(\nu_s)] P_s^+ + a_{sp}(z, t) \\ \frac{\partial P_s^-}{\partial z} - \frac{1}{v_g^s} \frac{\partial P_s^-}{\partial t} = [-g_s(z, t) + \alpha(\nu_s)] P_s^- - a_{sp}(z, t) \end{cases} \quad (3)$$

where

$$\begin{aligned} g_p(z, t) &= -\sigma_{12}(\nu_p) n_{1p}(z, t) + \sigma_{21}(\nu_p) n_{2p}(z, t), \\ g_s(z, t) &= -\sigma_{12}(\nu_s) n_{1s}(z, t) + \sigma_{21}(\nu_s) n_{2s}(z, t), \\ a_{sp}(z, t) &= 2h\nu_s B_{ase} \sigma_{21}(\nu_s) n_{2s}(z, t), \end{aligned}$$

are the gain coefficient for the pump, the gain coefficient for the signal and the spontaneous emission term, respectively, v_g^p and v_g^s are the group velocities for the pump and the signal, respectively, $\alpha(\nu)$ is the frequency-dependent optical loss of the glass and B_{ase} is the equivalent noise bandwidth for the Amplified Spontaneous Emission (ASE). The overlap integrals over the rare earth-doped region Ω_d between the ion populations and the pump/signal optical modes are calculated as follows:

$$\begin{aligned} n_{1p}(z, t) &= \int_{\Omega_d} N_1(x, y, z, t) i_p(x, y) dx dy \\ n_{2p}(z, t) &= \int_{\Omega_d} N_2(x, y, z, t) i_p(x, y) dx dy \\ n_{1s}(z, t) &= \int_{\Omega_d} N_1(x, y, z, t) i_s(x, y) dx dy \\ n_{2s}(z, t) &= \int_{\Omega_d} N_2(x, y, z, t) i_s(x, y) dx dy \end{aligned}$$

Therefore, the actual spatial distribution of both the ion population and the electromagnetic field is taken into account.

In order to solve the previous PDEs (3), suitable boundary and initial conditions are imposed (see Fig. 2):

$$\begin{aligned} P_p^+(0, t) &= P_{p0}^+(t) \\ P_p^-(L, t) &= P_{p0}^-(t) \\ P_s^+(0, t) &= R_1(\nu_s) P_s^-(0, t) \\ P_s^-(L, t) &= R_2(\nu_s) P_s^+(L, t) \end{aligned}$$

where $z = 0$ and $z = L$ represent the endpoints of the laser cavity, $P_{p0}^{\pm}(t)$ is the input forward/backward pump power signal, $R_1(\nu_s)$ is the first mirror reflectivity and $R_2(\nu_s)$ is the second mirror reflectivity. In addition, the system is considered to be initially at rest, therefore all rare earth ions are in the ground state and all the signals are zero everywhere:

$$N_1(x, y, z, 0) = N_{\text{Dy}}(x, y, z)$$

$$N_2(x, y, z, 0) = 0$$

$$P_p^+(z, 0) = P_p^-(z, 0) = P_s^+(z, 0) = P_s^-(z, 0) = 0$$

The time evolution of the generated optical pulses can be obtained as follows:

$$P_s^{\text{out}}(t) = [1 - R_2(\nu_s)]P_s^+(L, t) \quad (4)$$

III. NUMERICAL RESULTS

The fiber considered in the simulation is a step-index fluoride fiber, commercially available (Le Verre Fluoré), with core diameter $d_{\text{core}} = 12.5 \mu\text{m}$, cladding diameter $d_{\text{clad}} = 125 \mu\text{m}$ and numerical aperture $NA = 0.16$. The absorption and emission cross sections for the pump are $\sigma_{12}(\nu_p) = 3.26 \times 10^{-25} \text{ m}^2$ and $\sigma_{21}(\nu_p) = 2.04 \times 10^{-25} \text{ m}^2$, respectively. The absorption and emission cross sections for the signal are $\sigma_{12}(\nu_s) = 9.61 \times 10^{-26} \text{ m}^2$ and $\sigma_{21}(\nu_s) = 1.65 \times 10^{-25} \text{ m}^2$, respectively. The ${}^6\text{H}_{13/2} \rightarrow {}^6\text{H}_{15/2}$ radiative lifetime is $\tau_2 = 13.7 \text{ ms}$ and the ${}^6\text{H}_{13/2} \rightarrow {}^6\text{H}_{15/2}$ nonradiative decay rate is $R_{21} = 1539 \text{ s}^{-1}$. The equivalent ASE noise bandwidth is $B_{\text{ase}} = 100 \text{ nm}$. The glass refractive index is $n = 1.48$ at the wavelength $\lambda = 2.88 \mu\text{m}$. A suitable Sellmeier equation is considered to model the glass cladding refractive index dispersion, while keeping constant the numerical aperture NA . The group velocities for the pump and the signal are $v_g^p = 2.025 \times 10^8 \text{ m s}^{-1}$ and $v_g^s = 2.027 \times 10^8 \text{ m s}^{-1}$, respectively. They are very close, as expected. The optical losses are assumed to be equal to $\alpha = 0.9 \text{ dB m}^{-1}$ at both pump and signal wavelengths, i.e., high enough to include potential losses due to the splicing of the different parts of the laser cavity. The dopant concentration is $N_{\text{Dy}} = 2000 \text{ ppm} = 3.63 \times 10^{25} \text{ ions/m}^3$. The first mirror reflectivity is $R_1 = 99\%$. The pump and signal wavelengths are $\lambda_p = 2.8 \mu\text{m}$ and $\lambda_s = 3.0 \mu\text{m}$, respectively. The input pump peak power is $P_p^{\text{peak}} = 5 \text{ W}$. The time step size is $\Delta t = 5 \text{ ns}$ and the space step size is $\Delta z = 1 \text{ cm}$. In the following, the excitation pump waveform is assumed to be a square wave with variable amplitude, repetition rate and duty cycle. The time-dependent model has been validated by considering, as particular case, input pump power pulses with duty cycle $D = 100\%$, i.e., CW operation. All the parameters of the laser experimental set-up reported in [29] have been considered. By supposing a realistic coupling efficiency of about 30%, an output laser power very close to the experimental one has been obtained, with an agreement within 5%.

As an example of time-dependent simulation, Fig. 3 shows the unstable output signal pulses and the input pump pulses as a function of the time, input pump duty cycle $D = 40\%$, laser cavity length $L = 1 \text{ m}$ and second mirror reflectivity

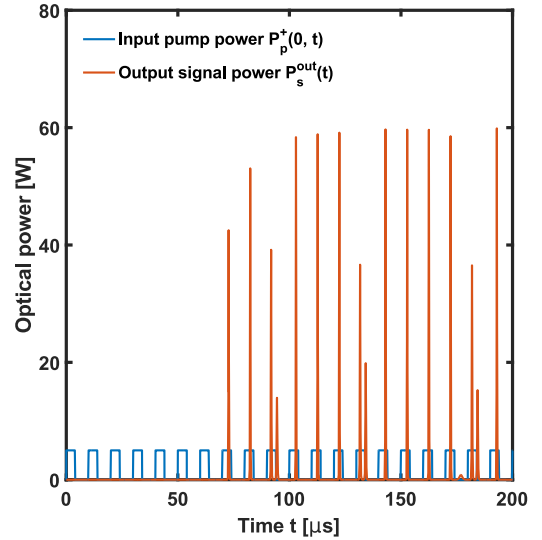


Fig. 3. Input pump power pulses $P_p^+(0, t)$ (blue pulses) and output signal power pulses $P_s^{\text{out}}(t)$ (red pulses) as a function of the time. Input pump duty cycle $D = 40\%$, laser cavity length $L = 1 \text{ m}$, pump repetition rate $f_R = 100 \text{ kHz}$, second mirror reflectivity $R_2 = 50\%$.

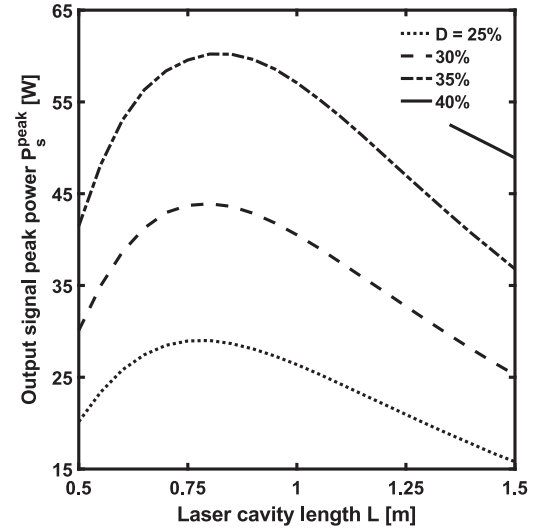


Fig. 4. Output signal peak power P_s^{peak} as a function of the cavity length L for different input pump duty cycles, $D = 25\%$ (dotted curve), $D = 30\%$ (dashed curve), $D = 35\%$ (dash-dot curve), $D = 40\%$ (solid curve). Pump repetition rate $f_R = 100 \text{ kHz}$; second mirror reflectivity $R_2 = 50\%$.

$R_2 = 50\%$. It is apparent that a proper design of the laser is mandatory in order to obtain stable single-pulse emission.

The output laser characteristics are investigated as a function of: i) laser cavity length L , see Figs. 4–6; ii) second mirror reflectivity R_2 , see Figs. 7–9; iii) input pump duty cycle D , see Figs. 10–12. Only points belonging to single-pulse stability regions are shown.

Fig. 4 shows the output signal peak power P_s^{peak} as a function of the laser cavity length L for different input pump duty cycles. The curves exhibit an increasing behavior for small cavity lengths, they reach the maximum for $L = 0.8 \text{ m}$ and then they decrease by increasing the cavity length. In other words,

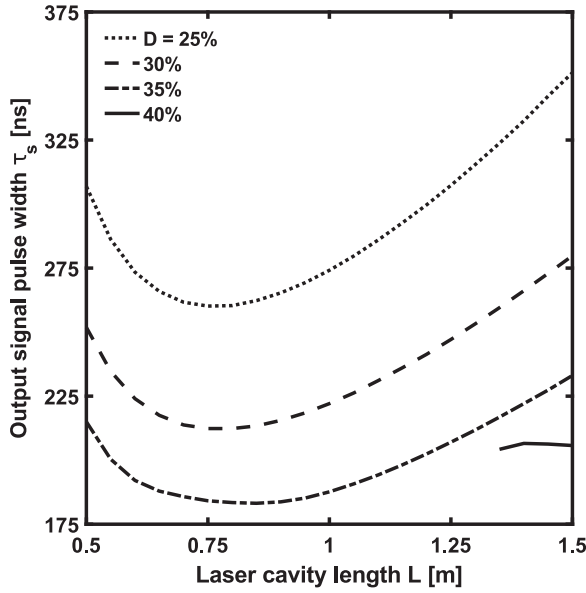


Fig. 5. Output signal pulse width τ_s as a function of the cavity length L for different input pump duty cycles, $D = 25\%$ (dotted curve), $D = 30\%$ (dashed curve), $D = 35\%$ (dash-dot curve), $D = 40\%$ (solid curve). Pump repetition rate $f_R = 100$ kHz; second mirror reflectivity $R_2 = 50\%$.

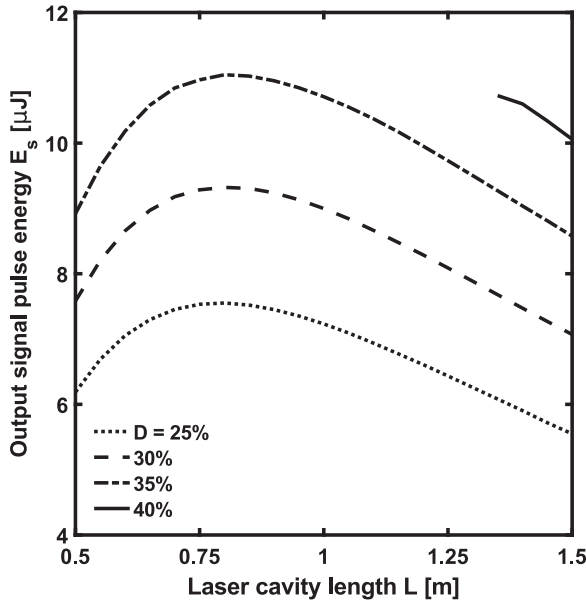


Fig. 6. Output signal pulse energy E_s as a function of the cavity length L for different input pump duty cycles, $D = 25\%$ (dotted curve), $D = 30\%$ (dashed curve), $D = 35\%$ (dash-dot curve), $D = 40\%$ (solid curve). Pump repetition rate $f_R = 100$ kHz; second mirror reflectivity $R_2 = 50\%$.

for a given laser configuration and dopant concentration, even by changing the average input pump power by considering different duty cycle values, the length $L = 0.8$ m seems to be the optimal one.

Fig. 5 shows the output signal pulse width τ_s as a function of the laser cavity length L for different input pump duty cycles. The simulation parameters are the same of Fig. 4. For short fibers, the pulse width exhibits a decreasing behavior and reaches a minimum at $L = 0.75$ - 0.85 m, then it increases. The

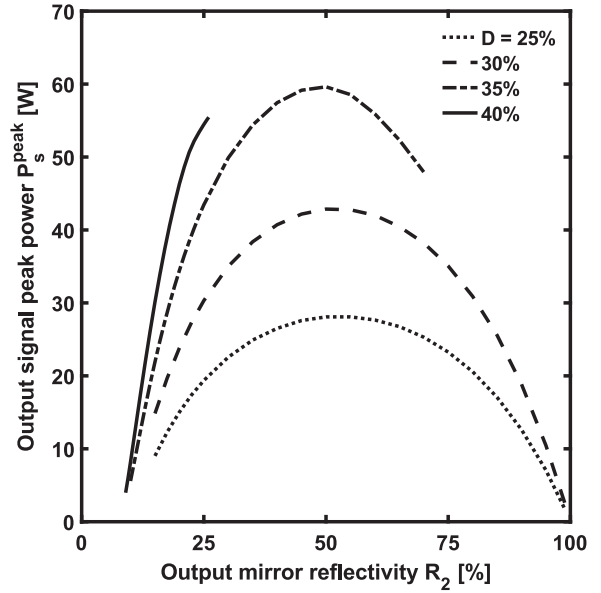


Fig. 7. Output signal peak power P_s^{peak} as a function of the output mirror reflectivity R_2 for different input pump duty cycles, $D = 25\%$ (dotted curve), $D = 30\%$ (dashed curve), $D = 35\%$ (dash-dot curve), $D = 40\%$ (solid curve). Pump repetition rate $f_R = 100$ kHz; cavity length $L = 0.9$ m.

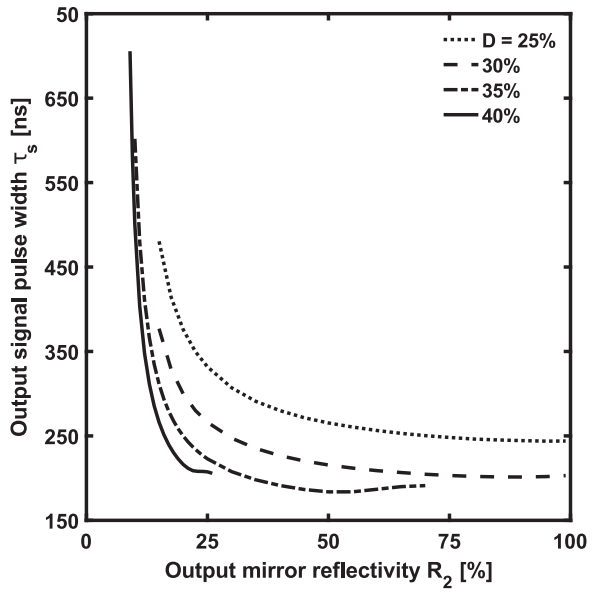


Fig. 8. Output signal pulse width τ_s as a function of the output mirror reflectivity R_2 for different input pump duty cycles, $D = 25\%$ (dotted curve), $D = 30\%$ (dashed curve), $D = 35\%$ (dash-dot curve), $D = 40\%$ (solid curve). Pump repetition rate $f_R = 100$ kHz; cavity length $L = 0.9$ m.

shortest achievable duration is about $\tau_s = 180$ ns, for $D = 35\%$. For $D = 40\%$, the performance deteriorates due to the stability region limited by non-optimal cavity lengths. The related pulse energy E_s is shown in Fig. 6. The maximum achievable pulse energy is about $E_s = 11$ μJ , for $D = 35\%$, leading to an optical-to-optical efficiency higher than $\eta = 60\%$.

Fig. 7 shows the output signal peak power P_s^{peak} as a function of the output mirror reflectivity R_2 for different input pump duty cycles. The curves exhibit an increasing behavior for low

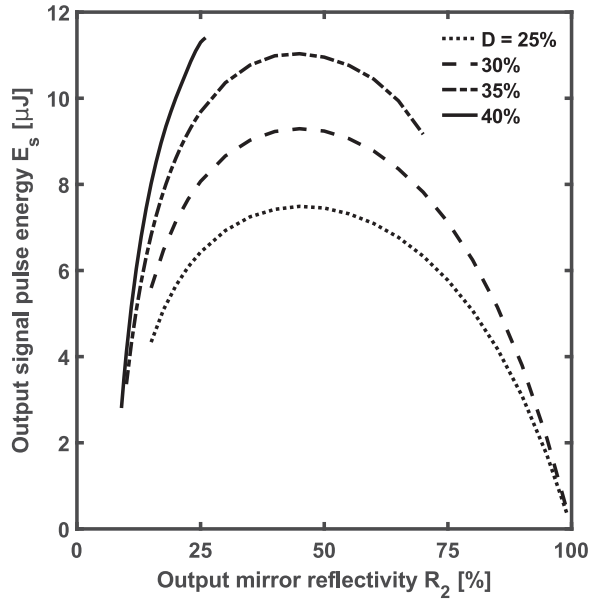


Fig. 9. Output signal pulse energy E_s as a function of the output mirror reflectivity R_2 for different input pump duty cycles, $D = 25\%$ (dotted curve), $D = 30\%$ (dashed curve), $D = 35\%$ (dash-dot curve), $D = 40\%$ (solid curve). Pump repetition rate $f_R = 100$ kHz; cavity length $L = 0.9$ m.

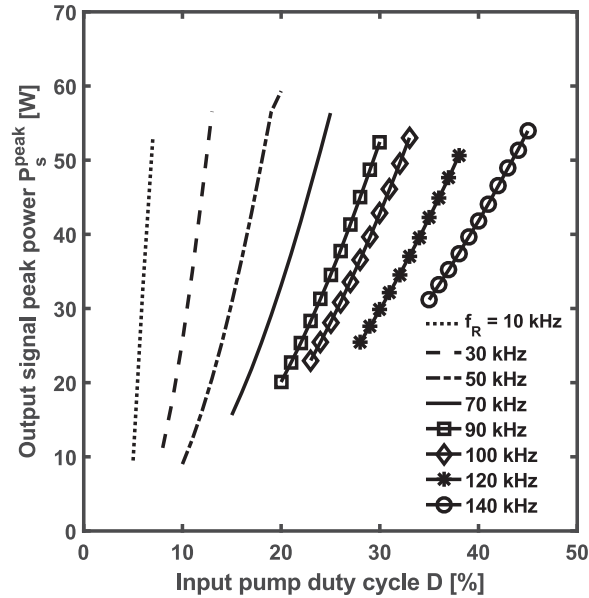


Fig. 10. Output signal peak power P_s^{peak} as a function of input pump duty cycle D for different pump repetition rates, $f_R = 10$ kHz (dotted curve), $f_R = 30$ kHz (dashed curve), $f_R = 50$ kHz (dash-dot curve), $f_R = 70$ kHz (solid curve), $f_R = 90$ kHz (solid curve with square markers), $f_R = 100$ kHz (solid curve with diamond markers), $f_R = 120$ kHz (solid curve with asterisk markers), $f_R = 140$ kHz (solid curve with circle markers). Cavity length $L = 0.9$ m; second mirror reflectivity $R_2 = 50\%$.

reflectivities and a decreasing behavior for high reflectivities. The maximum is reached around $R_2 = 50\%$, even if the pump duty cycle changes from $D = 25\%$ to $D = 35\%$. It is worthwhile noting that, for higher pump duty cycles, the single-pulse stability region gets narrower and narrower.

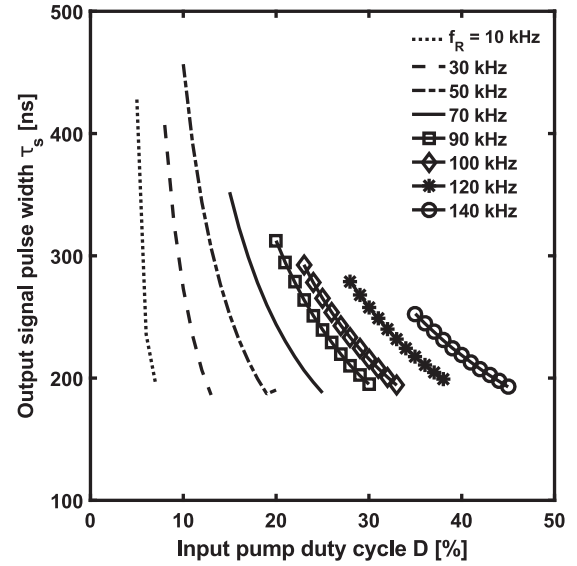


Fig. 11. Output signal pulse width τ_s as a function of input pump duty cycle D for different pump repetition rates, $f_R = 10$ kHz (dotted curve), $f_R = 30$ kHz (dashed curve), $f_R = 50$ kHz (dash-dot curve), $f_R = 70$ kHz (solid curve), $f_R = 90$ kHz (solid curve with square markers), $f_R = 100$ kHz (solid curve with diamond markers), $f_R = 120$ kHz (solid curve with asterisk markers), $f_R = 140$ kHz (solid curve with circle markers). Cavity length $L = 0.9$ m; second mirror reflectivity $R_2 = 50\%$.

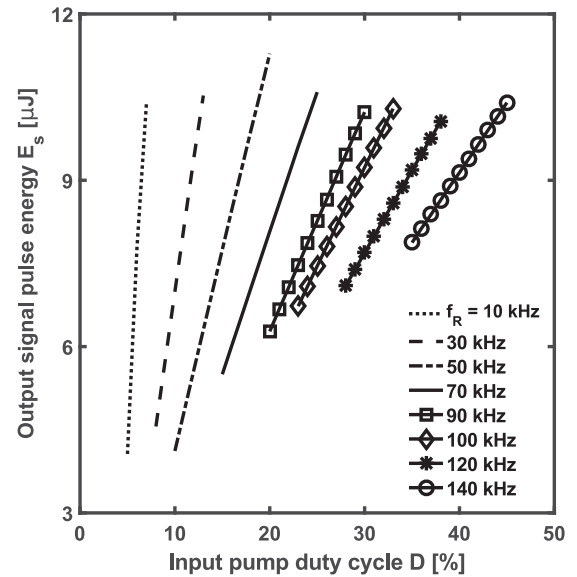


Fig. 12. Output signal pulse energy E_s as a function of input pump duty cycle D for different pump repetition rates, $f_R = 10$ kHz (dotted curve), $f_R = 30$ kHz (dashed curve), $f_R = 50$ kHz (dash-dot curve), $f_R = 70$ kHz (solid curve), $f_R = 90$ kHz (solid curve with square markers), $f_R = 100$ kHz (solid curve with diamond markers), $f_R = 120$ kHz (solid curve with asterisk markers), $f_R = 140$ kHz (solid curve with circle markers). Cavity length $L = 0.9$ m; second mirror reflectivity $R_2 = 50\%$.

Fig. 8 shows the output signal pulse width τ_s as a function of the output mirror reflectivity R_2 for different input pump duty cycles. The simulation parameters are the same of Fig. 7. The curves exhibit a monotone decreasing behavior, with a very steep slope for low reflectivities. For reflectivities greater than $R_2 = 40\%$, the pulse width is almost constant. Again, the best value

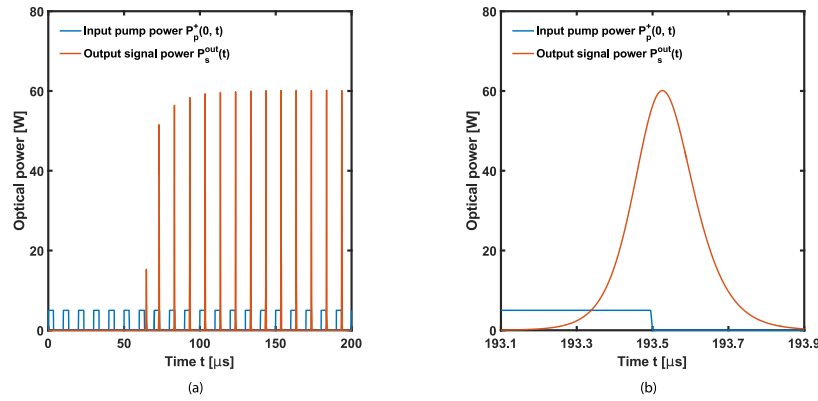


Fig. 13. (a) Input pump power pulses $P_p^+(0, t)$ (blue pulses) and output signal power pulses $P_s^{\text{out}}(t)$ (red pulses) as a function of the time. Input pump duty cycle $D = 35\%$, laser cavity length $L = 0.8$ m, pump repetition rate $f_R = 100$ kHz, second mirror reflectivity $R_2 = 50\%$. (b) Zoom of a single output signal pulse.

of about $\tau_s = 180$ ns is obtained for $R_2 = 50\%$, for the case $D = 35\%$. Fig. 9 shows the related pulse energy E_s . Like the previous case, the behavior is similar to that of Fig. 7, although the maximum pulse energy is obtained for $D = 40\%$.

Fig. 10 depicts the output signal peak power P_s^{peak} as a function of the input pump duty cycle D for different pump repetition rates. It is worthwhile noting that these curves refer to the average signal power, defined as $P_s^{\text{avg}} = E_s f_R$, varying from $P_s^{\text{avg}} = 0.04$ W to $P_s^{\text{avg}} = 1.45$ W and represent the regions in which stable output pulses are generated. It can be seen that a repetition rate as high as $f_R = 140$ kHz is feasible.

Fig. 11 shows the output signal pulse width τ_s as a function of the input pump duty cycle D for different pump repetition rates, for the same simulation parameters of Fig. 10. The curves are monotone decreasing for all repetition rate values, with a slope less and less steep as the repetition rate increases. In addition, the pulse width never falls below $\tau_s = 180$ ns. This is probably due to an inherent limitation of this fiber laser in gain switching operation. Also in this case, the pulse energy E_s , which is shown in Fig. 12, exhibits a behavior similar to that of the pulse peak power. Energies of about $E_s = 10$ – 11 μJ can be achieved for each value of the repetition rate, which provides great flexibility in the design of the device for both low and high repetition rates applications.

Figs. 10–12 are obtained for nearly optimized cavity length L and second mirror reflectivity R_2 and allow identifying the maximum pulse peak power P_s^{peak} , width τ_s and energy E_s achievable by varying the operating condition in terms of repetition rate f_R and duty cycle D .

Fig. 13(a) reports the generated pulses for the optimized laser, showing the stable output signal pulses and the input pump pulses as a function of the time, input pump duty cycle $D = 35\%$, laser cavity length $L = 0.8$ m and second mirror reflectivity $R_2 = 50\%$. After a build-up time of about $t = 65$ μs , the first pulse is generated. Stable gain-switched pulsed regime with an output peak power of $P_s^{\text{peak}} = 59$ W and a pulse duration of $\tau_s = 184$ ns, corresponding to an output energy of $E_s = 11$ μJ , is obtained after $t = 110$ μs . Fig. 13(b) depicts a zoom of a single output signal pulse.

The obtained results are promising, even with reference to the state of the art [28], [35], [36]. As examples, the following

characteristics of gain switched lasers were reported in the recent literature: i) in [35], pulse trains at $\lambda = 2.8$ μm with a maximum peak power of $P_s^{\text{peak}} = 68$ W, a duration of $\tau_s = 300$ ns and a pulse energy of $E_s = 20.4$ μJ at the repetition rate of $f_R = 100$ kHz in an Er^{3+} -doped ZBLAN fiber laser; ii) in [28], pulse trains at $\lambda = 2.8$ μm with a maximum peak power of $P_s^{\text{peak}} = 3.85$ W, a duration of $\tau_s = 1.55$ μs and a pulse energy of $E_s = 5.97$ μJ at the repetition rate of $f_R = 20$ kHz in the same fiber; iii) in [36], pulse trains at $\lambda = 2.98$ μm with a maximum peak power of $P_s^{\text{peak}} = 3.26$ W, a duration of $\tau_s = 1.49$ μs and a pulse energy of $E_s = 4.87$ μJ at the repetition rate of $f_R = 80$ kHz in a Ho^{3+} -doped ZBLAN fiber. In view of these results, the proposed ZBLAN fiber laser doped with Dy^{3+} ions constitutes an attractive solution since it allows the generation of pulse trains at $\lambda = 3$ μm with a maximum peak power of $P_s^{\text{peak}} = 59$ W, a duration of $\tau_s = 184$ ns, a pulse energy of $E_s = 11$ μJ and an optical-to-optical efficiency of $\eta = 60\%$ at the repetition rate of $f_R = 100$ kHz. Moreover, the proposed solution promises stable gain-switching operation even at higher repetition rates, e.g., at $f_R = 140$ kHz.

IV. CONCLUSION

For the first time, a Dy^{3+} :ZBLAN fiber laser operating in gain switching regime is accurately modeled and numerically investigated. By employing an input pump of 5 W with 100 kHz repetition rate and 35% duty cycle, pulses with a peak power of 59 W and a full width at half maximum (FWHM) width of 184 ns can be obtained. The related energy is 11 μJ , which corresponds to an optical-to-optical efficiency larger than 60%. The parameters of a commercially available fluoride fiber are used. Therefore, the proposed investigation can be considered a feasibility investigation of a pulsed laser which can be constructed by employing fluoride fibers available on the market.

REFERENCES

- [1] R. S. Quimby, L. B. Shaw, J. S. Sanghera, and I. D. Aggarwal, "Modeling of cascade lasing in Dy : Chalcogenide glass fiber laser with efficient output at 4.5 μm ," *IEEE Photon. Technol. Lett.*, vol. 20, no. 2, pp. 123–125, Jan. 2008.
- [2] D. D. Hudson, "Short pulse generation in mid-IR fiber lasers," *Opt. Fiber Technol.*, vol. 20, no. 6, pp. 631–641, Dec. 2014.

- [3] F. Starecki *et al.*, "Mid-IR optical sensor for CO₂ detection based on fluorescence absorbance of Dy^{3+} : Ga₅Ge₂₀Sb₁₀S₆₅ fibers," *Sens. Actuator B, Chem.*, vol. 207, Part A, no. 5, pp. 518–525, Sep. 2015.
- [4] M. C. Falconi *et al.*, "Design of an efficient pumping scheme for mid-IR Dy^{3+} : Ga₅Ge₂₀Sb₁₀S₆₅ PCF fiber laser," *IEEE Photon. Technol. Lett.*, vol. 28, no. 18, pp. 1984–1987, Sep. 2016.
- [5] L. Sojka *et al.*, "Numerical and experimental investigation of mid-infrared laser action in resonantly pumped Pt^{3+} doped chalcogenide fibre," *Opt. Quant. Electron.*, vol. 49, no. 1, Dec. 2016, Art. no. 21.
- [6] M. C. Falconi *et al.*, "Dysprosium-doped chalcogenide master oscillator power amplifier (MOPA) for mid-IR emission," *J. Lightw. Technol.*, vol. 35, no. 2, pp. 265–273, Jan. 2017.
- [7] G. Palma *et al.*, "Design of praseodymium-doped chalcogenide micro-disk emitting at 4.7 μm ," *Opt. Express*, vol. 25, no. 6, pp. 7014–7030, Mar. 2017.
- [8] L. Sojka *et al.*, "Mid-infrared emission in Tb^{3+} -doped selenide glass fiber," *J. Opt. Soc. Amer. B*, vol. 34, no. 3, pp. A70–A79, Mar. 2017.
- [9] L. Huang, S. Shen, and A. Jha, "Near infrared spectroscopic investigation of Tm^{3+} - Yb^{3+} co-doped tellurite glasses," *J. Non-Cryst. Solids*, vol. 345–346, pp. 349–353, Oct. 2004.
- [10] B. Richards, Y. Tsang, D. Binks, J. Lousteau, and A. Jha, "Efficient $\sim 2 \mu\text{m}$ Tm^{3+} -doped tellurite fiber laser," *Opt. Lett.*, vol. 33, no. 4, pp. 402–404, Feb. 2008.
- [11] L. Gomes, J. Lousteau, D. Milanese, E. Mura, and S. D. Jackson, "Spectroscopy of mid-infrared (2.9 μm) fluorescence and energy transfer in Dy^{3+} -doped tellurite glasses," *J. Opt. Soc. Amer. B*, vol. 31, no. 3, pp. 429–435, Mar. 2014.
- [12] R. Allen, L. Esterowitz, and R. J. Ginther, "Diode-pumped single-mode fluorozirconate fiber laser from the $^4I_{11/2} \rightarrow ^4I_{13/2}$ transition in erbium," *Appl. Phys. Lett.*, vol. 56, no. 17, pp. 1635–1637, 1990.
- [13] H. Yanagita, I. Masuda, T. Yamashita, and H. Toratani, "Diode laser pumped Er^{3+} fibre laser operation between 2.7–2.8 μm ," *Electron. Lett.*, vol. 26, no. 22, pp. 1836–1838, Oct. 1990.
- [14] R. M. Percival, S. F. Carter, D. Szebesta, S. T. Davey, and W. A. Stallard, "Thulium-doped monomode fluoride fibre laser broadly tunable from 2.25 to 2.5 μm ," *Electron. Lett.*, vol. 27, no. 21, pp. 1912–1913, Oct. 1991.
- [15] E. Poppe and B. Srinivasan, and R. K. Jain, "980 nm diode-pumped continuous wave mid-IR (2.7 μm) fibre laser," *Electron. Lett.*, vol. 34, no. 24, pp. 2331–2333, Nov. 1998.
- [16] S. D. Jackson, "Single-transverse-mode 2.5-W holmium-doped fluoride fiber laser operating at 2.86 μm ," *Opt. Lett.*, vol. 29, no. 4, pp. 334–336, Feb. 2004.
- [17] K. J. Linden, "Fiber laser with 1.2-W CW-output power at 2712 nm," *IEEE Photon. Technol. Lett.*, vol. 16, no. 2, pp. 401–403, Feb. 2004.
- [18] X. Zhu and R. Jain, "Compact 2 W wavelength-tunable Er:ZBLAN mid-infrared fiber laser," *Opt. Lett.*, vol. 32, no. 16, pp. 2381–2383, Aug. 2007.
- [19] S. Tokita, M. Hirokane, M. Murakami, S. Shimizu, M. Hashida, and S. Sakabe, "Stable 10 W Er:ZBLAN fiber laser operating at 2.71–2.88 μm ," *Opt. Lett.*, vol. 35, no. 23, pp. 3943–3945, Dec. 2010.
- [20] D. Faucher, M. Bernier, G. Androz, N. Caron, and R. Vallee, "20 W passively cooled single-mode all-fiber laser at 2.8 μm ," *Opt. Lett.*, vol. 36, no. 7, pp. 1104–1106, Apr. 2011.
- [21] S. D. Jackson, M. Pollnau, and J. Li, "Diode pumped erbium cascade fiber lasers," *IEEE J. Quantum Electron.*, vol. 47, no. 4, pp. 471–478, Apr. 2011.
- [22] R. Li, J. Li, L. Shterengas, and S. D. Jackson, "Highly efficient holmium fibre laser diode pumped at 1.94 μm ," *Electron. Lett.*, vol. 47, no. 19, pp. 1089–1090, Sep. 2011.
- [23] J. Li, L. Wang, H. Luo, J. Xie, and Y. Liu, "High power cascaded erbium doped fluoride fiber laser at room temperature," *IEEE Photon. Technol. Lett.*, vol. 28, no. 6, pp. 673–676, Mar. 2016.
- [24] J. Liu *et al.*, "Widely wavelength-tunable mid-infrared fluoride fiber lasers," *IEEE J. Sel. Topics Quantum Electron.*, vol. 24, no. 3, pp. 1–7, May 2018.
- [25] S. Antipov, D. D. Hudson, A. Fuerbach, and S. D. Jackson, "High-power mid-infrared femtosecond fiber laser in the water vapor transmission window," *Optica*, vol. 3, no. 12, pp. 1373–1376, Dec. 2016.
- [26] J. Yang, Y. Tang, R. Zhang, and J. Xu, "Modeling and characteristics of gain-switched diode-pumped Er-Yb codoped fiber lasers," *IEEE J. Quantum Electron.*, vol. 48, no. 12, pp. 1560–1567, Dec. 2012.
- [27] S. Yan *et al.*, "Developing high-power hybrid resonant gain-switched thulium fiber lasers," *Opt. Express*, vol. 23, no. 20, pp. 25675–25687, Oct. 2015.
- [28] C. Wei, H. Luo, H. Shi, Y. Lyu, H. Zhang, and Y. Liu, "Widely wavelength tunable gain-switched Er^{3+} -doped ZBLAN fiber laser around 2.8 μm ," *Opt. Express*, vol. 25, no. 8, pp. 8816–8827, Apr. 2017.
- [29] M. R. Majewski and S. D. Jackson, "Highly efficient mid-infrared dysprosium fiber laser," *Opt. Lett.*, vol. 41, no. 10, pp. 2173–2176, May 2016.
- [30] M. R. Majewski and S. D. Jackson, "Tunable dysprosium laser," *Opt. Lett.*, vol. 41, no. 19, pp. 4496–4498, Oct. 2016.
- [31] M. R. Majewski, R. I. Woodward, and S. D. Jackson, "Dysprosium-doped ZBLAN fiber laser tunable from 2.8 μm to 3.4 μm , pumped at 1.7 μm ," *Opt. Lett.*, vol. 43, no. 5, pp. 971–974, Mar. 2018.
- [32] R. I. Woodward, M. R. Majewski, G. Bharathan, D. D. Hudson, A. Fuerbach, and S. D. Jackson, "Watt-level dysprosium fiber laser at 3.15 μm with 73% slope efficiency," *Opt. Lett.*, vol. 43, no. 7, pp. 1471–1474, Apr. 2018.
- [33] J. Yang, H. Li, Y. Tang, and J. Xu, "Temporal characteristics of in-band-pumped gain-switched thulium-doped fiber lasers," *J. Opt. Soc. Amer. B*, vol. 31, no. 1, pp. 80–86, Jan. 2014.
- [34] R. J. LeVeque, *Finite Difference Methods for Ordinary and Partial Differential Equations: Steady-State and Time-Dependent Problems*. Philadelphia, PA, USA: SIAM, 2007.
- [35] M. Gorjan, R. Petkovsek, M. Marinček, and M. Copic, "High-power pulsed diode-pumped Er:ZBLAN fiber laser," *Opt. Lett.*, vol. 36, no. 10, pp. 1923–1925, May 2011.
- [36] H. Luo, J. Li, Y. Hai, X. Lai, and Y. Liu, "State-switchable and wavelength-tunable gain-switched mid-infrared fiber laser in the wavelength region around 2.94 μm ," *Opt. Express*, vol. 26, no. 1, pp. 63–79, Jan. 2018.

Mario Christian Falconi (S'14) received the M.Sc. degree in electronic engineering (*cum laude*) in 2015 from the Polytechnic University of Bari, Bari, Italy, where he is currently working toward the Ph.D. degree in electrical and information engineering. His research interests include fiber lasers and amplifiers, photonic crystal fibers, and nonlinear effects in optical fibers.

Dario Laneve received the M.Sc. degree in information engineering (*cum laude*) in 2014 from the Polytechnic University of Bari, Bari, Italy, where he is currently working toward the Ph.D. degree in electrical and information engineering. His research interests include microwave resonators for linear accelerators and optical resonators for sensing applications.

Michele Bozzetti received the M.Sc. degree in electronic engineering (*cum laude*) in 1975. He is an Associate Professor of electromagnetic fields and head of the Electromagnetic Compatibility Laboratory, Polytechnic University of Bari, Bari, Italy.

Toney Teddy Fernandez received the Ph.D. degree in 2009 from Mahatma Gandhi University, Kerala, India. He joined the Department of Physics, Polytechnic of Milan, Milan, Italy from 2015 until 2018 and is currently Senior Researcher with MQ Photonics, Department of Physics and Astronomy, Macquarie University, Sydney, NSW, Australia. His area of interests include amorphous materials, ultrafast light-matter interaction, and mid-infrared light sources.

Gianluca Galzerano received the Ph.D. degree in metrology from the Polytechnic of Turin, Torino, Italy, in 1999. Since 2001, he has been a Researcher with the Institute for Photonics and Nanotechnology, National Research Council (IFN-CNR), Rome, Italy, and an Adjunct Professor with the Polytechnic of Milan, Milano, Italy. From April 2010 to November 2013, he was the Director of the IFN-CNR. His research includes the development of solid-state lasers and amplifiers, based on innovative materials and techniques, widely tunable in the near- and mid-infrared spectral region. He has coauthored 230 publications on international journals and conferences, lectures, and invited papers.

Francesco Prudeniano received the Ph.D. degree in electronic engineering in November 1996. Since 2003, he has been an Associate Professor in electromagnetic fields with the Department of Electrical and Information Engineering, Polytechnic University of Bari, Bari, Italy. His research activity regards the design and characterization of microwave devices, integrated optics, and optical fiber-based devices. He is chair of SIOF, the Italian Society of Optics and Photonics (Italian branch of European Optical Society). He is involved in several national and international research projects and cooperations. He has coauthored more than 380 publications, 285 of which published on journals and international conferences, lectures, and invited papers.